Effects of Protonation State on a Tyrosine–Histidine Bioinspired Redox Mediator

ARTICLE *in* THE JOURNAL OF PHYSICAL CHEMISTRY B · NOVEMBER 2010

Impact Factor: 3.3 · DOI: 10.1021/jp101592m · Source: PubMed

Effects of Protonation State on a Tyrosine−Histidine Bioinspired Redox Mediator†

Gary F. Moore,‡,# Michael Hambourger,§ Gerdenis Kodis,‡ Weston Michl,‡ Devens Gust,*,‡ Thomas A. Moore,*,‡ and Ana L. Moore*,‡

Center for Bioenergy and Photosynthesis and Department of Chemistry and Biochemistry, Arizona State University, Tempe, Arizona 85287-1604, and A. R. Smith Department of Chemistry, Appalachian State University, Boone, North Carolina 28608

Received: February 22, 2010; Revised Manuscript Received: April 24, 2010

The conversion of tyrosine to the corresponding tyrosyl radical in photosytem II (PSII) is an example of proton-coupled electron transfer. Although the tyrosine moiety (Tyr_Z) is known to function as a redox mediator between the photo-oxidized primary donor ($P680^{\bullet+}$) and the Mn-containing oxygen-evolving complex, the protonation states involved in the course of the reaction remain an active area of investigation. Herein, we report on the optical, structural, and electrochemical properties of tyrosine−histidine constructs, which model the function of their naturally occurring counterparts in PSII. Electrochemical studies show that the phenoxyl/phenol couple of the model is chemically reversible and thermodynamically capable of water oxidation. Studies under acidic and basic conditions provide clear evidence that an ionizable proton controls the electrochemical potential of the tyrosine−histidine mimic and that an exogenous base or acid can be used to generate a low-potential or high-potential mediator, respectively. The phenoxyl/phenoxide couple associated with the low-potential mediator is thermodynamically incapable of water oxidation, whereas the relay associated with the high-potential mediator is thermodynamically incapable of reducing an attached photoexcited porphyrin. These studies provide insight regarding the mechanistic role of the tyrosine−histidine complex in water oxidation and strategies for making use of hydrogen bonds to affect the coupling between proton and electron transfer in artificial photosynthetic systems.

Introduction

Biology offers inspiration for designing energy transduction schemes that use solar energy (reaching Earth's surface at a rate of ∼120,000 TW) to meet global human energy demands (∼15 TW).[1−11] Application of these concepts will require effective coupling of light capture, photochemical charge separation, and efficient catalysts in order to use solar energy to harvest a sustainable source of electrons (i.e., water) for the production of a reduced fuel. In photosynthesis, solar energy conversion involves spatial separation of the light capture, charge separation, and catalytic centers responsible for energy storage in chemical bonds.[12,13] Charge-separating reaction centers are organized so that redox shuttles carry electrons to catalysts for the reduction of protons or carbon-based coenzymes; in photosystem II, the holes are transported to a tetramanganese cluster, which oxidizes water to molecular oxygen and protons. A biological membrane, protein structures, and molecular recognition between redox centers ensures vectorial charge flow and prevents short circuits between high-potential and low-potential carriers. In this system, the inherent single-electron photochemistry of the primary donor (P680) is interfaced with multielectron catalytic reactions via single-electron mediators.[14−16] This fundamental aspect of natural photosynthesis will likely be of importance in artificial constructs seeking to mimic oxygenic photosynthesis.

In PSII, the tyrosyl/tyrosine redox couple mediates charge transport between the photo-oxidized primary donor ($P680^{\bullet+}$) and the Mn-containing oxygen-evolving complex (OEC) during the Kok−Joliot S-state cycle.[17,18] An important aspect of the electron transfer from tyrosine (Tyr_Z) to $P680^{\bullet+}$ (and from the OEC to the tyrosyl radical) is the coupling of proton chemistry with redox reactions. The oxidation of Tyr_Z likely occurs with release of the phenolic proton to a nearby base (presumably the hydrogen-bonded histidine residue, His190);[19−21] the oxidation is coupled to a change in pK_a from 10 to −2.[22−29] Reduction of the tyrosyl radical by the OEC is likewise coupled to the return of a proton. Indeed, such proton-coupled electron-transfer (PCET) reactions appear fundamental to many biological energy transduction schemes.[30−34]

Model systems involving closely associated phenol-based moieties are one means of gaining insight into the complex interactions of the Tyr_Z−His190 pair in PSII.[35−44] We have recently reported a photochemically active mimic of the chlorophyll−Tyr_Z−His190 complex of PSII.[45] In this bioinspired system, a chlorophyll-like species, a modified bis(pentafluorophenylporphyrin), is attached to both a phenol−benzimidazole pair (Tyr_Z−His190 mimic) and a titanium dioxide nanoparticle electron acceptor. Light excitation of the porphyrin triggers the rapid injection of an electron into the conduction band of the semiconductor. The resulting charge-separated state ($P^{\bullet+}$−$TiO_2^{\bullet-}$) undergoes a secondary charge shift reaction by transferring a hole from the oxidized porphyrin to the phenol−benzimidazole. The resulting stable phenoxyl radical is thermodynamically poised for water oxidization.

Herein, we report a detailed structural, electrochemical, and optical study of a model phenol−benzimidazole (**1**) and its methoxy derivative (**2**) (see Chart 1). Investigation of these

† Part of the "Michael R. Wasielewski Festschrift".

* To whom correspondence should be addressed. E-mail: gust@asu.edu (D.G.); tmoore@asu.edu (T.A.M.); amoore@asu.edu (A.L.M.).

‡ Arizona State University.

§ Appalachian State University.

Current address: Department of Chemistry, Yale University, P.O. Box 208107, New Haven, CT 06520-8107.

10.1021/jp101592m
Published on Web 05/17/2010

CHART 1: Compounds 1−4

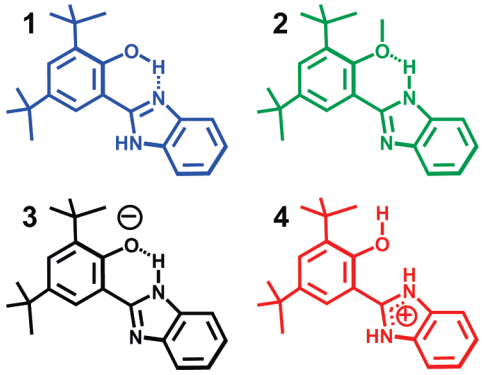

CHART 2: Compounds 5−7

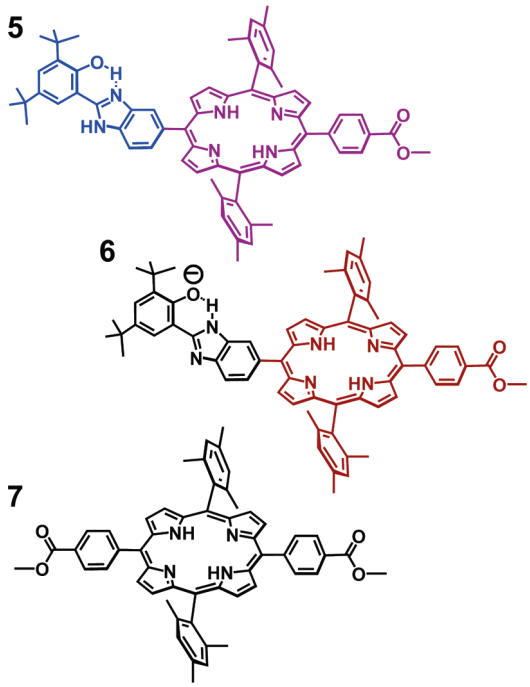

compounds in organic solvents under neutral, acidic, and basic conditions provides insight regarding the role of the phenol protonation state in charge mediation. Further, we report a (mesitylporphyrin)-bearing analogue (**5**) (see Chart 2) in which the photoexcited porphyrin is not sufficiently oxidizing to remove an electron from the covalently attached phenol−benzimidazole pair. However, the addition of base to a solution of **5** removes the phenolic proton, and the resulting phenoxide acts as an effective electron donor to the first singlet excited state of the porphyrin. While the phenoxyl/phenoxide couple associated with this process is capable of reducing the attached porphyrin chromophore, the redox couple is thermodynamically incapable of water oxidization at a biologically relevant pH.

These results provide clear evidence that an ionizable proton controls the electrochemical potential of the phenolic species and that an exogenous base or acid can be used to generate a low-potential or high-potential mediator, respectively, while maintaining the chemical reversibility of the system. These studies provide insight regarding the coupling of proton transfer to a hydrogen-bonded base as a strategy for tuning the redox potential of an electron mediator.

Experimental Section

All chemicals were purchased from Aldrich, Acros, or Alfa Aesar. Solvents were obtained from EM Science. Toluene was distilled over CaH_2, and dichloromethane was distilled over potassium carbonate. All solvents were stored over the appropriate molecular sieves prior to use. All compounds were synthesized from commercially available starting materials (see Supporting Information (SI), Synthesis and Structural Characterization). Thin-layer chromatography (TLC) was performed with silica-gel-coated glass plates from Analtech. Column chromatography was carried out using Silicycle silica gel 60, 230−400 mesh. The ^{1}H NMR spectra were recorded on Varian spectrometers at 300, 400, or 500 MHz. NMR samples were prepared in deuteriochloroform, benzene-d_6, or dimethylsulfoxide-d_6 with tetramethylsilane as an internal reference. Mass spectra were obtained with a matrix-assisted laser desorption/ionization time-of-flight spectrometer (MALDI-TOF).

Steady-state absorbance spectra were measured on a Shimadzu UV-3101PC UV−vis−NIR spectrometer. Steady-state fluorescence spectra were measured using a Photon Technology International MP-1 spectrometer and corrected for detection system response. Excitation was provided by a 75 W xenon arc lamp and single grating monochromator. Fluorescence was detected 90° to the excitation beam via a single grating monochromator and an R928 photomultiplier tube having S-20 spectral response and operating in the single-photon counting mode. Time-resolved fluorescence decay measurements were performed by the time-correlated single-photon counting method (see SI, Time-Resolved Fluorescence Measurements).

Data were obtained in either dichloromethane or toluene. In situ generation of protonated and/or deprotonated forms of **1**, **2**, **5**, **7**, and **8** was achieved by the addition of acid or base, respectively, under a nitrogen atmosphere. Either trifluoroacetic acid (TFA) or gaseous HCl was used as the acid. Either solid tetramethylammonium hydroxide (TMAOH) or a methanolic solution of tetrabutylammonium hydroxide (TBAOH) was used as the base. For acid−base titrations in toluene, a solution of TFA in toluene or TBAOH in methanol was used. For in situ formation of protonated or deprotonated species in dichloromethane, gaseous HCl was used as the acid, and solid TMAOH was used as the base (see SI, Synthetic Section).

Cyclic voltammetry was performed with a CHI 650C potentiostat (CH Instruments) using a glassy carbon (3 mm diameter) or platinum disk (1.6 mm diameter) working electrode, a platinum gauze counter electrode, and a silver wire pseudoreference electrode in a conventional three-electrode cell. Anhydrous dichloromethane stored over potassium carbonate, or benzonitrile distilled from phosphorus pentoxide, was used as the solvent for electrochemical measurements. In both cases, the supporting electrolyte was 0.10 M tetrabutylammonium hexafluorophosphate, and the solution was deoxygenated by bubbling with argon. The working electrode was cleaned between experiments by polishing with an alumina slurry, followed by solvent rinses. The concentration of the electroactive compound was maintained between 4×10^{-4} and 8×10^{-4} M. In some instances (experiments involving the addition of base or acid in dichloromethane solutions), cyclic voltammetry was performed at 1 °C. Acidified dichloromethane was made by adding a stock solution (in the same solvent) of TFA to a final concentration up to 0.5 M. Basified dichloromethane was made by adding solid TMAOH until the solution was saturated. The potential of the pseudoreference electrode was determined using the ferrocenium/ferrocene redox couple as an internal standard (with $E_{1/2}$ taken as 0.45 V versus SCE in dichloromethane). The voltammograms were recorded at 100 mV s^{-1}. Cyclic voltammograms obtained at a glassy carbon working electrode have the baseline subtracted, using a baseline recorded under

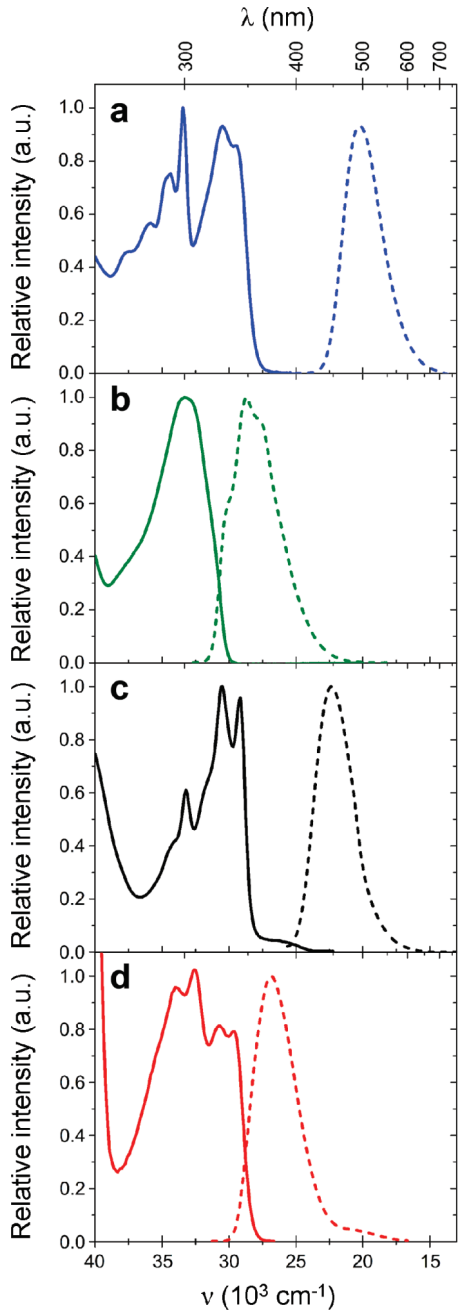

Figure 1. Steady-state absorption (solid lines) and emission (dashed lines) spectra of (a) **1** and (b) **2** in dichloromethane, as well as **1** in dichloromethane after the addition of excess (c) tetramethylammonium hydroxide, shifting the equilibrium to favor the deprotonated species **3** or (d) gaseous HCl, giving rise to the protonated species **4**.

comparable conditions in the absence of the electroactive species. All potentials listed in this article are referenced to the saturated calomel electrode (SCE).

Results

Steady-State Optical Studies. To investigate the acid−base equilibria of **1**, we measured the steady-state absorption and emission spectra of compounds **1** and **2**, along with those of the deprotonated (**3**) and protonated (**4**) forms of **1** (Figure 1). In dichloromethane, the absorption spectrum of **1** exhibits fine structure, with peaks at 266, 279, 291, 299, 328, and 339 nm. The emission spectrum of **1** reveals a substantial Stokes shift of 155 nm, with $\lambda_{max} = 494$ nm. In comparison, the absorption

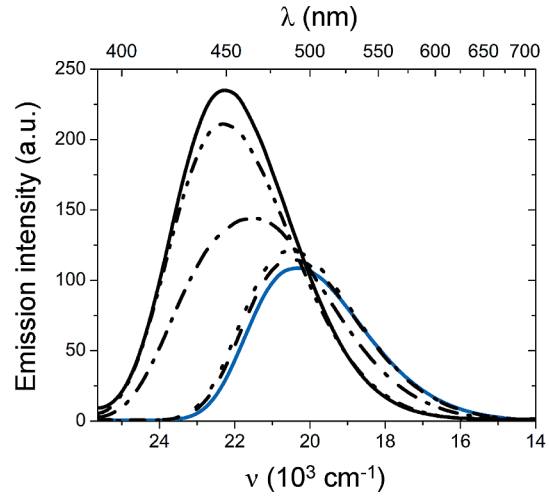

Figure 2. Steady-state emission spectra (320 nm excitation) of **1** in toluene (initially 2.7 mL of 6×10^{-6} M) (blue solid line) and upon sequential additions of 100 μL aliquots of methanolic solutions of TBAOH at concentrations of 1×10^{-4} (dashed line), 1×10^{-3} (dotted line), 0.01 (dash−dot line), 0.1 (dash−dot−dot line), and 1 M (black solid line).

of the methoxy derivative (**2**) ($\lambda_{max} = 300$ nm) is substantially blue-shifted relative to **1** and without fine structure. The emission of **2** ($\lambda_{max} = 348$ nm) displays a more modest Stokes shift of 48 nm. Upon treatment of **1** with a base (TMAOH), the absorbance maxima are altered, with a low-intensity band appearing at longer wavelengths. The emission spectrum of the deprotonated species is substantially blue-shifted ($\lambda_{max} = 447$ nm) compared to the neutral form (**1**). Upon treatment of **1** with acid (HCl), the absorption spectrum exhibits changes, and the emission spectrum is blue-shifted ($\lambda_{max} = 372$ nm) compared to **1** in neat dichloromethane. In contrast to compound **1**, treatment of **2** with excess base does not change the absorption properties (see SI, Figure S1). However, treatment of **2** with acid (HCl) results in a small shift to longer wavelengths in the absorbance maximum ($\lambda_{max} = 307$ nm) and a larger shift in the emission maximum ($\lambda_{max} = 388$ nm) (see SI, Figure S2). Similar absorption and emission spectra were observed in toluene using methanolic solutions of tetrabutylammonium hydroxide or trifluoroacetic acid (see SI, Figure S3).

Additional information was obtained by titration of **1** with aliquots of tetrabutylammonium hydroxide (TBAOH) in methanol. In toluene, this titration series results in a hypsochromic shift of the emission spectra from $\lambda_{max} = 493$ to 449 nm (Figure 2). Treatment of the resulting basic solution with acetic acid returns the emission spectrum to its original form, with a slight hypsochromic shift in the emission attributed to the addition of methanol (see SI, Figures S5 and S6). Titration of **1** in toluene with aliquots of trifluoroacetic acid (TFA) also results in a large hypsochromic shift of the emission spectrum, with $\lambda_{max} = 388$ nm (see SI, Figure S7). In contrast, emission spectra of **1** recorded in ethanol are identical ($\lambda_{max} = 477$ nm) in the presence and absence of acid (see SI, Figure S8).

The UV−vis absorption studies of a solution of **1** under basic or acidic conditions reveal the presence of two acid−base equilibria. In keeping with previous interpretations of the acid−base equilibria of phenol−benzimidazole pairs,[46,47] we postulate that treatment of **1** with base or acid produces the anionic species (**3**) or the cationic species (**4**), respectively. In the case of **1**, the large Stokes shift suggests that the initially formed excited state is not the same species that gives rise to the emission. Due to the inherent change in pK_a of the excited

state[48,49] and the close proximity of the phenolic hydroxyl group to the nitrogen lone pair of the attached benzimidazole, it is inferred that **1** undergoes an excited-state intramolecular proton transfer (ESIPT),[50] forming a zwitterionic keto species,[46,47,50] which exhibits a red-shifted fluorescence (see SI, Figure S10, and Figure 1).[45]

Titration of **1** with base shifts the ground-state equilibrium to strongly favor the deprotonated phenoxide ion, resulting in a hypsochromic shift of the fluorescence spectrum with emission from the higher-energy excited state of the anionic species **3**. Under acidic conditions, the neutral species **1** is converted into the cationic species **4** via protonation of the benzimidazole base. Shifting the equilibrium to favor **4** precludes excited-state proton transfer to the benzimidazole base, as observed for **1**, giving rise to a higher-energy emission spectrum in acidified toluene. This is not the case for the emission spectra of **1** recorded in ethanol (SI, Figure S8) where the addition of acid causes no spectral shift, an effect that can be attributed to deprotonation of the excited phenol to the bulk solution.

The methoxy derivative **2** is incapable of undergoing ESIPT. Hence, titration of **2** with TFA results in a bathochromic shift of the emission spectra (SI, Figure S9). In addition, the concentration of acid required to induce changes in the optical spectrum of **2** is considerably less than that required for **1**. This likely reflects the increase in basicity of **2** relative to **1**, an effect that can be attributed to a difference in the internal H-bonded structures as shown in Chart 1 (see next section).

Nuclear Magnetic Resonance Studies. Structural features of compounds **1** and **2**, as well as the deprotonated and protonated forms of **1** generated in situ by the addition of base (TMAOH) or acid (a gaseous stream of HCl), respectively, were elucidated using nuclear magnetic resonance (^{1}H NMR). The OH resonance in **1** (14.20 ppm in benzene-d_6) represents a strongly deshielded phenolic proton, indicative of a hydrogen bond. The benzimidazole NH resonance of **2** (9.46 ppm in benzene-d_6) is shifted downfield with respect to the benzimidazole NH of compound **1** ($\Delta\delta$ = 1.41 ppm), indicative of a more electronegative environment for this proton. For the deprotonated and protonated forms of **1**, trace quantities of methanol-d_4 were required to dissolve the ionic species in acidified or basified benzene-d_6. Under these experimental conditions, the OH and NH protons exchange with the solvent, and their resonances could not be observed.

Information regarding the local electrostatic environment of the 4′ and 6′ protons provides insight into the relative orientations of the phenol and benzimidazole ring systems. Assignments of the 4′ and 6′ resonances are based on NOESY measurements of the through-space dipolar coupling of these nuclei with the neighboring *tert*-butyl protons, which appear in the aliphatic region of the ^{1}H NMR spectra recorded in benzene-d_6 (Figure 3 and Figure S14, SI). For **1**, the aromatic 4′ and 6′ protons of the phenol appear as meta-coupled doublets (J = 2.5 Hz) at 7.64 and 7.05 ppm, respectively. The spectrum of **2** is markedly different, with the 6′ resonance appearing at 8.61 ppm ($\Delta\delta$ = 1.56 ppm relative to **1**). The deprotonated species, generated by treatment of **1** with base, displays a similar downfield shift of the 6′ resonance (δ = 8.35 ppm; $\Delta\delta$ = 1.30 ppm with respect to **1**). The protonated species, formed by the addition of acid to **1**, also displays a downfield shift of the 6′ resonance (δ = 7.58 ppm; $\Delta\delta$ = 0.53 ppm with respect to **1**) but to a much lesser extent than that for the deprotonated species or for compound **2**. The chemical shifts of the 4′ resonances in compounds **1** and **2** are essentially identical as they are in the deprotonated and protonated forms of **1**. Full assignments of the ^{1}H NMR spectra based on COSY and NOESY experiments in benzene-d_6 and chloroform-d are provided in the SI (Figures S14−S16).

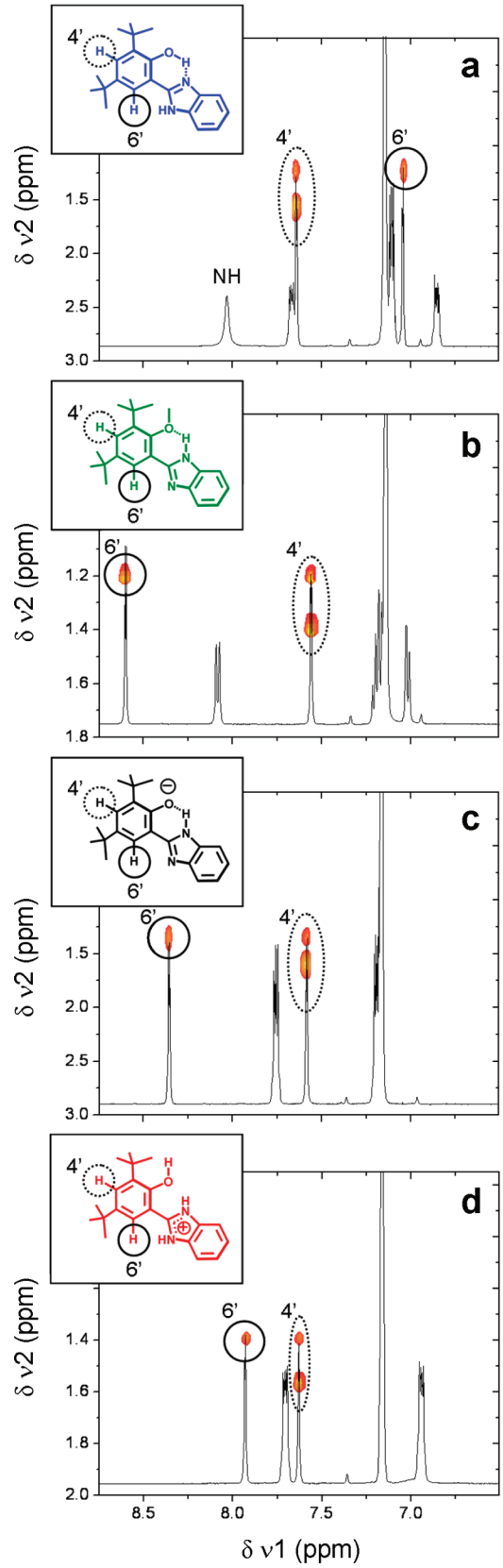

Figure 3. 400 MHz NOSEY and overlaid ^{1}H NMR spectra in benzene-d_6 of (a) **1** and (b) **2**, as well as **1** under (c) basic and (d) acidic conditions.

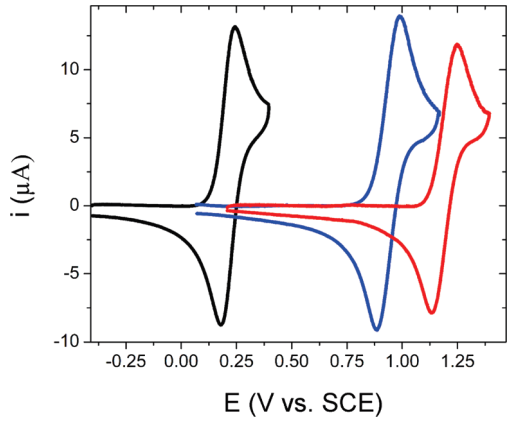

Figure 4. Cyclic voltammograms recorded at a glassy carbon electrode for a 1 mM solution of **1** in dichloromethane (blue line) and upon addition of excess tetramethylammonium hydroxide (black line) or trifluoroacetic acid (red line) (see Experimental Section). Together, these voltammograms indicate that the protonation state of the phenol−benzimidazole influences the electrochemical behavior, but the one-electron oxidation remains chemically reversible under both acidic and basic conditions.

The presence of an intramolecular hydrogen bond in **1** and **2** is supported by the ^{1}H NMR spectra, which show the downfield-shifted phenolic OH resonance of **1** at 14.20 ppm and the downfield-shifted benzimidazole NH resonance of **2** at 9.46 ppm in benzene-d_6. However, the nature of these hydrogen bonds is drastically different, as inferred from comparison of the 4′ and 6′ resonances of the phenol (Figure 3). In the case of **1**, the phenolic proton forms a hydrogen bond with the lone pair electrons of the benzimidazole. In this structure, the 6′ proton (7.05 ppm) faces the benzimidazole NH proton. In contrast, in **2**, the benzimidazole ring is rotated relative to the phenol with the NH proton of the benzimidazole forming a hydrogen bond with the oxygen lone pair of the methoxy substituent. Consequently, the 6′ proton is deshielded due primarily to a through-space electrostatic field effect from the nitrogen lone pair (8.61 ppm) in **2**, as compared to **1**.[51] On the basis of the NMR data, we further postulate that the deprotonated species **3** is also stabilized by a hydrogen bond between the NH proton of the benzimidazole and the oxygen lone pair of the phenoxide. The large downfield shift of the meta-coupled doublet at the 6′ position is consistent with this interpretation. In the protonated species, **4**, the change in the chemical shift of the aromatic 6′ proton with respect to its shift in **1** is rationalized in terms of an inductive/field effect caused by the formal positive charge of the attached benzimidazolium cation. Although the presence of an internal H-bond in compound **4** seems likely, by analogy with the other compounds studied here, the NMR spectra are inconclusive with respect to such. Therefore, no internal H-bond is indicated in the structure of **4**, as illustrated in Chart 1.

Electrochemical Studies. The protonation state of the phenol−benzimidazole has a major influence on its electrochemical properties. For **1** in dichloromethane, a reversible one-electron oxidation is observed with a midpoint potential of 0.94 V versus SCE (Figure 4). The addition of base (TMAOH) results in a reversible, one-electron oxidation at 0.21 V versus SCE, at the expense of the 0.94 V feature. In contrast, the addition of acid (TFA) to neutral **1** results in an anodic shift of the one-electron oxidation to 1.19 V versus SCE. An irreversible oxidation (E_p = 1.46 V versus SCE) is the only redox process observed in dichloromethane for **2**, which lacks the phenol moiety.

SCHEME 1: Structures Associated with the Reduced and Oxidized Forms of 1 and 3 and the Corresponding $E_{1/2}$ (V versus SCE)

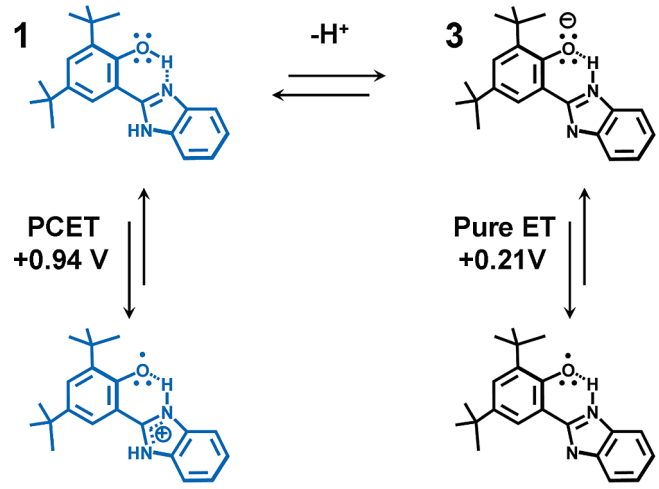

The electrochemical behavior of the phenol−benzimidazole pair (**1**) differs from that of model compounds such as 2,4-di-*tert*-butylphenol (E_p = 1.37 V versus SCE), 2,4,6-tri-*tert*-butylphenol (E_p = 1.36 V versus SCE), or benzimidazole (E_p = 1.59 V versus SCE) in dichloromethane. In these compounds, the oxidation is irreversible and only observed at higher potentials than the first oxidation of **1**. The electrochemistry of 2,4,6-tri-*tert*-butylphenol has been previously reported under neutral and basic conditions in acetonitrile.[52] Results obtained in our laboratory in dichloromethane (with and without the addition of TMAOH) are consistent with this previous report.

The observed electrochemistry of **1** is consistent with previous reports of this species in organic solvents.[38,45] Unlike the typical electrochemistry of phenols (which are notoriously irreversible and known to exhibit two-electron oxidations),[52] the one-electron oxidation of **1** is chemically reversible (Figure 4). This behavior is attributed to a transfer of the phenolic proton to the attached benzimidazole upon oxidation, rather than to the bulk solution as is the case for 2,4,6-tri-*tert*-butylphenol.[45] In the case of **1**, the proton can toggle between the oxygen and nitrogen lone pair electrons in the corresponding reduced and oxidized forms with minimal nuclear motion, giving rise to stabilization of the one-electron oxidation product and the observed chemically reversible redox behavior (Scheme 1).

The electrochemical measurements indicate that the deprotonated species (**3**) also undergoes a chemically reversible one-electron oxidation. This process is cathodically shifted relative to that in the neutral species **1** ($\Delta E_{1/2}$ = 730 mV) due to the greater electron density on the phenoxide of **3** (Scheme 1). Interestingly, the protonated species **4** also undergoes a chemically reversible one-electron oxidation that is anodically shifted with respect to the neutral species **1**. The chemical reversibility of **4** may reflect proton-coupled electron transfer, forming the same one-electron oxidation product as that for **1**. Alternatively, the results may indicate a pure electron transfer, forming the phenol radical cation−benzimidazolium cation pair following the one-electron oxidation of **4**. Although the formation of the dicationic species seems unlikely, the present data do not allow us to definitively distinguish between these two possibilities.

Optical and Electronic Properties of Porphyrin-Containing Systems. In order to study the photochemical generation of phenolic radicals, compound **5** was prepared. It contains both a phenol−benzimidazole and a porphyrin chromophore. The

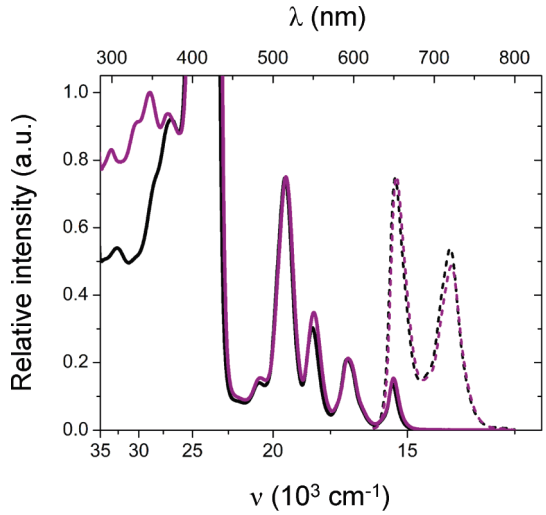

Figure 5. Steady-state absorption (solid lines) and emission (dashed lines) spectra of **5** (purple solid and dashed lines) and **7** (black solid and dashed lines) recorded in toluene.

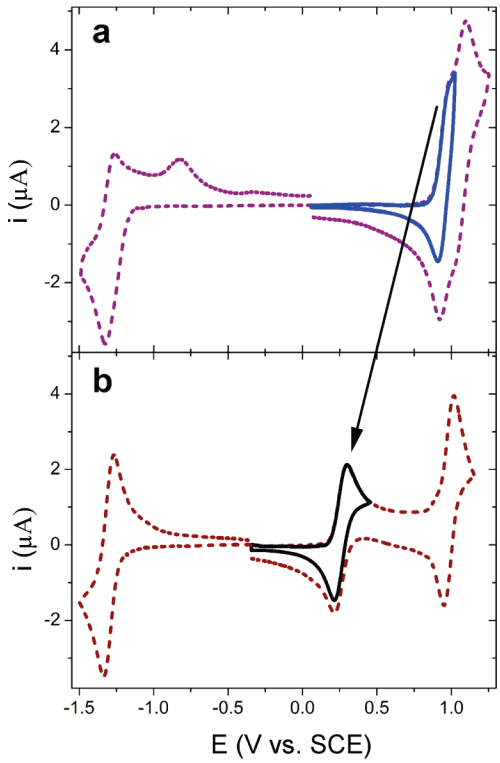

Figure 6. Cyclic voltammograms recorded at a glassy carbon electrode for (a) **5** in dichloromethane recorded from 0.06 to +1.03 V (solid blue line) and 0.06 to −1.49 V and 0.06 V to +1.25 V (dashed purple lines) as well as (b) an identical solution in the presence of excess TMAOH recorded from −0.35 to +0.46 V (solid black line) and from −0.35 to −1.50 and −0.35 to +1.16 V (dashed brown lines).

absorption spectrum of **5** is nearly identical to that of porphyrin **7**, with the exception of additional spectral features in the ultraviolet region similar to those observed for compound **1** (Figure 5). Likewise, the cyclic voltammograms of **5** exhibit features characteristic of the individual constituents (Figure 6). Visible excitation (555 nm) of **5** or **7** results in emission spectra typical of a free base porphyrin macrocycle (with emission maxima in toluene at 653 and 721 nm for **5** and 652 and 720 nm for **7**). Titration of **5** in toluene with successive aliquots of TBAOH in methanol results in quenching of the porphyrin singlet excited-state emission (Figure 7), with fluorescence

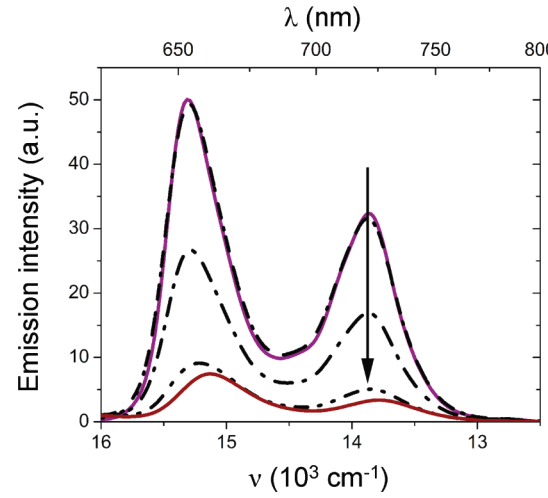

Figure 7. Steady-state emission spectra (555 nm excitation) of **5** in toluene (initially 2.7 mL of a 6×10^{-6} M solution, purple solid line) and upon sequential additions of 100 μL aliquots of methanolic solutions of TBAOH at concentrations of 1×10^{-4} (dashed line), 1×10^{-3} (dotted line), 0.01 (dash−dot line), 0.1 (dash−dot−dot line), and 1 M (brown solid line).

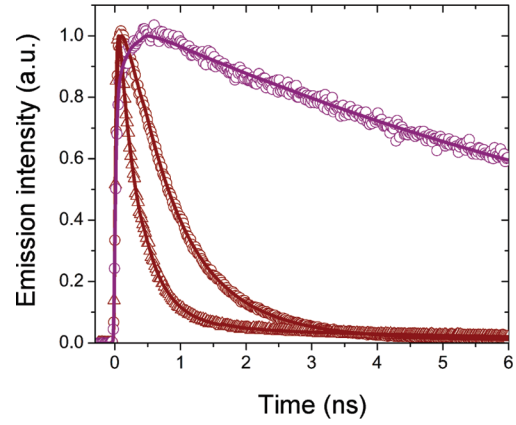

Figure 8. Time-resolved fluorescence single-photon counting (SPC) measurements of **5** in toluene (purple circles), in toluene basified with TBAOH (brown circles), in methyl THF basified with TBAOH (brown triangles), and the kinetic fitting of the data (solid lines).

quenching occurring at essentially the same concentrations of base that were required to deprotonate the model phenol **1** (Figure 1). The addition of sufficient TBAOH to a solution of **5** in toluene quenches the steady-state fluorescence to ∼15% of the original value, and the emission spectrum is slightly red-shifted. In contrast, titration of **7** in toluene with successive aliquots of TBAOH results in negligible change in the absorption and emission spectra (see SI, Figure S13).

Fluorescence quenching of **5** in the presence of base was quantified by time-resolved fluorescence single-photon counting (SPC) measurements, which show a porphyrin singlet excited-state lifetime for **5** in neat toluene of 10.32 ns and lifetimes of 630 ps (70% component) and 1.18 ns (30% component) upon the addition of TBAOH to the solution (Figure 8). For comparison, the porphyrin singlet excited-state lifetime of model compound **7** is ∼10 ns. In 2-methyltetrahydrofuran (methyl THF), a solvent more polar than toluene, the addition of base to a solution of **5** results in even greater quenching of the porphyrin singlet excited state, with the lifetime reduced to 160 (60% component) and 420 ps (40% component). The two lifetime components may be associated with the presence of distinct 1,3-tautomeric forms of the benzimidazole−phenoxide (Bi−PhO:$^-$) moiety in **6**.

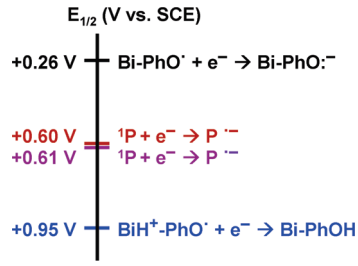

Figure 9. Energy level diagram for compounds **5** and **6** showing the $E_{1/2}$ for the $^1P/P^{\bullet -}$ process in compounds **5** (purple) and **6** (brown), the phenoxyl/phenol couple of **5** (Bi−PhOH) (blue), and the phenoxyl/phenoxide of **6** (Bi−PhO:$^-$) (black).

Optical studies of **5**, **6**, and **7** indicate that the porphyrin singlet excited state can oxidize the low-potential phenoxide species but not the higher-potential phenol (Figures 7 and 8). This is consistent with the estimated potential for the $^1P/P^{\bullet -}$process (0.61 and 0.60 V versus SCE for **5** and **6**, respectively) (see SI, Electrochemical Data), which has a potential lower than that of the phenoxyl/phenol couple of **5** at 0.95 V versus SCE yet higher than that of the phenoxyl/phenoxide couple at 0.26 V versus SCE. In this case, reductive electron transfer from the benzimidazole−phenol (Bi−PhOH) to the excited porphyrin is endergonic ($\Delta G_{ET} \approx 340$ meV), while the electron transfer from the deprotonated species (the benzimidazole−phenoxide, Bi−PhO:$^-$) is exergonic ($\Delta G_{ET} \approx -340$ meV) (Figure 9). The quenching of the porphyrin excited state upon the addition of base indicates newly accessible deactivation pathways for the excited state, namely, electron transfer from the attached phenoxide−benzimidazole pair to the porphyrin singlet excited state. On the basis of the fluorescence lifetime data, the quantum yield of phenoxyl radical formation is >90% in both solvents, benzene and THF.

Discussion

Comparisons with the Natural Photosynthetic Apparatus. It is interesting to compare these results to those obtained from studies of the natural photosynthetic apparatus using Mn-depleted PSII enriched membranes.[27,28,53] Faller and co-workers reported on the EPR properties of a trapped, high-energy intermediate radical formed during the oxidation of tyrosine D at liquid helium temperatures. Two possible mechanisms were proposed to describe the intermediate formed during the low-temperature photoinduced oxidation. One model consists of a PCET, in which the neutral tyrosine transfers its phenolic proton to the hydrogen-bonded nitrogen lone pair electrons of His189 upon oxidation. This forms the trapped intermediate state, in which the neutral tyrosyl radical is hydrogen-bonded to the histidinium cation. Upon warming, this intermediate state relaxes via deprotonation of the histidinium to a nearby residue.

The second mechanism involves a "pure electron transfer", process in which an initially deprotonated tyrosinate, hydrogen-bonded to the NH of the neutral His189 residue, is oxidized. In this model, oxidation involves only electron transfer (to the photo-oxidized $P680^{\bullet +}$), giving rise to a trapped intermediate in which the phenoxyl radical remains hydrogen-bonded to the NH proton of neutral His189. In this model, relaxation of the strained intermediate requires mainly an elongation of the hydrogen bond via a histidine motion upon warming. Given that this mechanism requires initial deprotonation of the reduced tyrosine (in the pH range where PSII is active, the tyrosine/tyrosinate equilibrium favors the protonated form in the reduced state),[54,55] the pure electron transfer mechanism can be viewed as a stepwise process proceeding via initial tyrosine deprotonation, followed by electron transfer, i.e., a proton-transfer electron-transfer (PTET) mechanism. Although Faller et al. favored the PCET mechanism, the pure electron transfer mechanism could not be ruled out by their data.

In recent efforts to further characterize the coupling of electron and proton motion involving the Tyr/His in PSII, Rappaport and co-workers have measured the kinetics of tyrosine oxidation in Mn-depleted PSII preparations in which the driving force for electron and/or proton transfer was altered by site-directed mutagenesis or substitution of tyrosine by a fluorinated analogue, respectively.[53] From their results, Rappaport and co-workers concluded that the reduction of $P680^{\bullet +}$ could involve a stepwise PTET mechanism in which $P680^{\bullet +}$ is reduced by the tyrosinate formed by proton transfer to a nearby base, in this case, the imidazole group of His190. This stepwise mechanism is not the same as the pure electron transfer mechanism described by Faller et al. because it results in formation of a salt bridge between the tyrosinate and the protonated base (the histidinium ion), rather than a hydrogen bond between the tyrosinate and the NH proton of a neutral histidine residue. This is an important distinction, given that the salt bridge probably would affect the potential of the tyrosyl/tyrosinate redox couple and other properties of the system.[53]

In previous work, we have invoked a PCET mechanism to describe the temperature-dependent steady-state distribution of trapped states observed by EPR following light excitation of a photoactive mimic of the chlorophyll−Tyr_Z−His190 complex of PSII.[45] In this system, photoinduced electron transfer coupled to proton motion at the phenolic site produces a stable phenoxyl radical that is thermodynamically capable of water oxidation. In the system reported herein, oxidation of the phenol moiety by the attached porphyrin in its singlet excited state is thermodynamically allowed only when the phenolic proton has been removed; the process is best described as a PTET. NMR studies indicate that the phenoxide forms a hydrogen bond with the attached benzimidazole NH proton and as such is a good model for the pure electron transfer mechanism of Faller et al. However, the phenoxyl/phenoxide couple of this system at 0.26 V versus SCE is thermodynamically incapable of water oxidation at a biologically relevant pH. Our observation that the oxidized form of the artificial Tyr/His couple could not oxidize water makes a strong argument against the stepwise mechanism involving a tyrosinate−histidine species of the pure electron-transfer mechanism. However, this conclusion cannot be extended to a stepwise mechanism involving a salt bridge tyrosinate−histidinium intermediate. The present work does not model that mechanism.

Conclusions

We have prepared a selection of bioinspired, photochemically active constructs consisting of a porphyrin covalently attached to phenol−benzimidazole moieties. Different protonation states of the phenol−benzimidazole were prepared by the addition of acids or bases. The neutral species that features an intramolecular hydrogen bond between the phenol and the lone pair of the imidazole is an effective high-potential mediator ($E_{1/2} = 0.95$ versus SCE), with redox characteristics comparable to those of the Tyr_Z of PSII, and mimics quite closely the electron-mediating role played by this redox active residue.[45] On the other hand, when the phenol is deprotonated by the addition of a strong base, even though the phenoxide ion remains hydrogen-bonded to the electrophilic NH of imidazole, it becomes a low-potential entity ($E_{1/2} = 0.26$ versus SCE) thermodynamically incapable

of promoting water oxidation. To the extent that these results reflect the behavior of the related moieties in the natural photosynthetic system, they suggest that the PTET mechanism is less likely than a PCET mechanism in water oxidation by PS II. The special case of PTET in which the proton is transferred to form the imidazolium ion[53] is not addressed by this work.

The model systems described in this work mimic aspects of their natural counterparts and provide a basis for a better mechanistic understanding of the role of the Tyr_Z−His190 pair in water oxidation, proton activity during charge transport, and potential strategies for minimizing nuclear reorganization and/or making use of hydrogen bonds to affect the coupling between proton and electron transfer in artificial systems.[56−62]

Acknowledgment. This work is supported as part of the Center for Bio-Inspired Solar Fuel Production, an Energy Frontier Research Center funded by the U.S. Department of Energy, Office of Science, Office of Basic Energy Sciences under Award Number DE-SC0001016. T.A.M. acknowledges the Blaise Pascal Research Chairs for support of work in biomimetic solar energy conversion in collaboration with groups at Université Paris-Sud, Orsay, and CEA Saclay. We thank Ally Aukauloo and A. William Rutherford for their insightful suggestions.

Supporting Information Available: Synthesis and structural characterization, steady-state optical data, time-resolved fluorescence, NMR data, optical data, and electrochemical data. This material is available free of charge via the Internet at http://pubs.acs.org.

References and Notes

(1) Lewis, N. S.; Nocera, D. G. *Proc. Natl. Acad. Sci., U.S.A.* **2006**, *103*, 15729–15735.
(2) Lubitz, W.; Reijerse, E. J.; Messinger, J. *Energy Environ. Sci.* **2008**, *1*, 15–31.
(3) Hambourger, M.; Moore, G. F.; Kramer, D. M.; Gust, D.; Moore, A. L.; Moore, T. A. *Chem. Soc. Rev.* **2009**, *38*, 25–35.
(4) Barber, J. *Chem. Soc. Rev.* **2009**, *38*, 185–196.
(5) Gust, D.; Moore, T. A.; Moore, A. L. *Acc. Chem. Res.* **2009**, *42*, 1890–1898.
(6) Gust, D.; Moore, T. A.; Moore, A. L. *Acc. Chem. Res.* **2001**, *34*, 40–48.
(7) Gust, D.; Moore, T. A.; Moore, A. L. *Acc. Chem. Res.* **1993**, *26*, 198–205.
(8) Wasielewski, M. R. *Chem. Rev.* **1992**, *92*, 435–461.
(9) Holten, D.; Bocian, D. F.; Lindsey, J. S. *Acc. Chem. Res.* **2002**, *35*, 57–69.
(10) Martin, N.; Sanchez, L.; Herranz, M. A.; Illescas, B.; Guldi, D. M. *Acc. Chem. Res.* **2007**, *40*, 1015–1024.
(11) Hammarström, L.; Sun, L.; Åkermark, B.; Styring, S. *Spectrochim. Acta, Part A* **2001**, *37*, 2145–2160.
(12) Yachandra, V. K.; Sauer, K.; Klein, M. P. *Chem. Rev.* **1996**, *96*, 2927–2950.
(13) Blankenship, R. E. *Molecular Mechanisms of Photosynthesis*; Blackwell Science, Ltd.: Malden, MA, 2002.
(14) McEvoy, J. P.; Brudvig, G. W. *Chem. Rev.* **2006**, *106*, 4455–4483.
(15) Brudvig, G. W. *Philos. Trans. R. Soc. London, Ser. B* **2008**, *363*, 1211–1219.
(16) Hammarström, L.; Styring, S. *Philos. Trans. R. Soc. London, Ser. B* **2008**, *363*, 1283–1291.
(17) Joliot, P.; Barbieri, G.; Chabaud, R. *Photochem. Photobiol.* **1969**, *10*, 309–329.
(18) Kok, B.; Forbush, B.; McGloin, M. *Photochem. Photobiol.* **1970**, *11*, 457–475.
(19) Harriman, A. *J. Phys. Chem.* **1987**, *91*, 6102–6104.
(20) Dixon, W. T.; Murphy, D. *J. Chem. Soc., Faraday Trans. 2* **1976**, *72*, 1221–1230.
(21) Rappaport, F.; Lavergne, J. *Biochemistry* **1997**, *36*, 15294–15302.
(22) Ahlbrink, R.; Haumann, M.; Cherepanov, D.; Boegershausen, O.; Mulkidjanian, A.; Junge, W. *Biochemistry* **1998**, *37*, 1131–1142.
(23) Hoganson, C. W.; Babcock, G. T. *Science* **1997**, *277*, 1953–1956.
(24) Hays, A.-M. A.; Vassiliev, I. R.; Golbeck, J. H.; Debus, R. J. *Biochemistry* **1999**, *38*, 11851–11865.
(25) Tommos, C.; Babcock, G. T. *Biochim. Biophys. Acta* **2000**, *1458*, 199–219.
(26) Meyer, T. J.; Huynh, M. H. V.; Thorp, H. H. *Angew. Chem., Int. Ed.* **2007**, *46*, 5284–5304.
(27) Faller, P.; Rutherford, A. W.; Debus, R. J. *Biochemistry* **2002**, *41*, 12914–12920.
(28) Faller, P.; Goussias, C.; Rutherford, A. W.; Un, S. *Proc. Natl. Acad. Sci. U.S.A.* **2003**, *100*, 8732–8735.
(29) Diner, B. A.; Force, D. A.; Randall, D. W.; Britt, R. D. *Biochemistry* **1998**, *37*, 17931–17943.
(30) Cukier, R. I.; Nocera, D. G. *Annu. Rev. Phys. Chem.* **1998**, *49*, 337–369.
(31) Hammes-Schiffer, S. *Acc. Chem. Res.* **2001**, *34*, 273–281.
(32) Stubbe, J.; Nocera, D. G.; Yee, C. S.; Chang, M. C. Y. *Chem. Rev.* **2003**, *103*, 2167–2201.
(33) Mayer, J. M. *Annu. Rev. Phys. Chem.* **2004**, *55*, 363–390.
(34) Huynh, M. H. V.; Meyer, T. J. *Chem. Rev.* **2007**, *107*, 5004–5064.
(35) Burdinski, D.; Wieghardt, K.; Steenken, S. *J. Am. Chem. Soc.* **1999**, *121*, 10781–10787.
(36) Sjödin, M.; Styring, S.; Åkermark, B.; Sun, L.; Hammarström, L. *J. Am. Chem. Soc.* **2000**, *122*, 3932–3936.
(37) Maki, T.; Araki, Y.; Ishida, Y.; Onomura, O.; Matsumura, Y. *J. Am. Chem. Soc.* **2001**, *123*, 3371–3372.
(38) Benisvy, L.; Bill, E.; Blake, A. J.; Collison, D.; Davies, E. S.; Garner, C. D.; Guindy, C. I.; McInnes, E. J. L.; McArdle, G.; McMaster, J.; Wilson, C.; Wolowska, J. *Dalton Trans.* **2004**, 3647–3653.
(39) Rhile, I. J.; Mayer, J. M. *J. Am. Chem. Soc.* **2004**, *126*, 12718–12719.
(40) Lachaud, F.; Quaranta, A.; Pellegrin, Y.; Dorlet, P.; Charlot, M.-F.; Un, S.; Leibl, W.; Aukauloo, A. *Angew. Chem., Int. Ed.* **2005**, *44*, 1536–1540.
(41) Costentin, C.; Robert, M.; Savéant, J.-M. *J. Am. Chem. Soc.* **2006**, *128*, 4552–4553.
(42) Rhile, I. J.; Markle, T. F.; Nagao, H.; DiPasquale, A. G.; Lam, O. P.; Lockwood, M. A.; Rotter, K.; Mayer, J. M. *J. Am. Chem. Soc.* **2006**, *128*, 6075–6088.
(43) Lomoth, R.; Magnuson, A.; Sjödin, M.; Huang, P.; Styring, S.; Hammarström, L. *Photosynth. Res.* **2006**, *87*, 25–40.
(44) Costentin, C.; Louault, C.; Robert, M.; Savéant, J.-M. *J. Am. Chem. Soc.* **2008**, *130*, 15817–15819.
(45) Moore, G. F.; Hambourger, M.; Gervaldo, M.; Poluektov, O. G.; Rajh, T.; Gust, D.; Moore, T. A.; Moore, A. L. *J. Am. Chem. Soc.* **2008**, *130*, 10466–10467.
(46) Mosquera, M.; Penedo, J. C.; Rodríguez, M. C. R.; Rodríguez-Prieto, F. *J. Phys. Chem.* **1996**, *100*, 5398–5407.
(47) Bräuer, M.; Mosquera, M.; Pérez-Lustres, J. L.; Rodríguez-Prieto, F. *J. Phys. Chem. A* **1998**, *102*, 10736–10745.
(48) Förster, T. *Naturwissenschaften* **1949**, *36*, 186–187.
(49) Weller, A. *Naturwissenschaften* **1955**, *42*, 175–176.
(50) Formosinho, S. J.; Arnaut, L. G. *J. Photochem. Photobiol., A* **1993**, *75*, 21–48.
(51) Hand, E. S.; Paudler, W. W. *Org. Magn. Reson.* **1980**, *14*, 52–54.
(52) Richards, J. A.; Whitson, P. E.; Evans, D. H. *J. Electroanal. Chem.* **1975**, *63*, 311–327.
(53) Rappaport, F.; Boussac, A.; Force, A. D.; Peloquin, J.; Brynda, M.; Sugiura, M.; Un, S.; Britt, R. D.; Diner, B. A. *J. Am. Chem. Soc.* **2009**, *131*, 4425–4433.
(54) Berthomieu, C.; Hienerwadel, R.; Boussac, A.; Breton, J.; Diner, B. A. *Biochemistry* **1998**, *37*, 10547–10554.
(55) Noguchi, T.; Inoue, Y.; Tang, X.-S. *Biochemistry* **1997**, *36*, 14705–14711.
(56) Cady, C. W.; Crabtree, R. H.; Brudvig, G. W. *Coord. Chem. Rev.* **2008**, *252*, 444–455.
(57) Hoertz, P. G.; Kim, Y.-I.; Youngblood, W. J.; Mallouk, T. E. *J. Phys. Chem. B* **2007**, *111*, 6845–6856.
(58) Kanan, M. W.; Nocera, D. G. *Science* **2008**, *321*, 1072–1075.
(59) Youngblood, W. J.; Lee, S.-H. A.; Kobayashi, Y.; Hernandez-Pagan, E. A.; Hoertz, P. G.; Moore, T. A.; Moore, A. L.; Gust, D.; Mallouk, T. E. *J. Am. Chem. Soc.* **2009**, *131*, 926–927.
(60) Le Goff, A.; Artero, V.; Jousselme, B.; Tran, P. D.; Guillet, N.; Métayé, R.; Fihri, A.; Palacin, S.; Fontecave, M. *Science* **2009**, *326*, 1384–1387.
(61) Woolerton, T. W.; Sheard, S.; Reisner, E.; Pierce, E.; Ragsdale, S. W.; Armstrong, F. A. *J. Am. Chem. Soc.* **2010**, *132*, 2132–2133.
(62) Brimblecombe, R.; Koo, A.; Dismukes, C.; Swiegers, G. R.; Spiccia, L. *J. Am. Chem. Soc.* **2010**, *132*, 2892–2894.

JP101592M